Magnetic anisotropy of chloritoid

Tom Haerinck,[1] Timothy N. Debacker,[2] and Manuel Sintubin [1]

Received 9 January 2013; revised 24 June 2013; accepted 28 June 2013; published 6 August 2013.

[1] The magnetocrystalline anisotropy of monoclinic chloritoid, a relatively common mineral in aluminum-rich, metapelitic rocks, has been determined for the first time by measuring the high-field anisotropy of magnetic susceptibility (HF-AMS), using two independent approaches, i.e., (a) directional magnetic hysteresis measurements and (b) torque magnetometry, on a collection of single crystals collected from different tectonometamorphic settings worldwide. Magnetic remanence experiments show that all specimens contain ferromagnetic (*s.l.*) impurities, being mainly magnetite. The determined HF-AMS ellipsoids have a highly oblate shape with the minimum susceptibility direction subparallel to the crystallographic c-axis of chloritoid. In the basal plane of chloritoid, though the HF-AMS can be considered isotropic. The degree of anisotropy is found to be 1.47, which is significantly higher than the anisotropy of most paramagnetic silicates and even well above the frequently used upper limit (i.e., 1.35) for the paramagnetic contribution to the AMS of siliciclastic rocks. The obtained values for the paramagnetic Curie temperature parallel ($\theta^{\parallel}$) and perpendicular ($\theta^{\perp}$) to the basal plane indicate that this pronounced magnetocrystalline anisotropy is related to strong antiferromagnetic exchange interactions in the direction of the crystallographic c-axis ($\theta^{\perp} < 0$) and rather weak ferromagnetic exchange interactions within the basal plane ($\theta^{\parallel} > 0$). As a consequence, chloritoid-bearing metapelites with a pronounced mineral alignment can have a high degree of anisotropy without the need of invoking a significant contribution of strongly anisotropic, ferromagnetic (*s.l.*) minerals. The newly discovered magnetocrystalline anisotropy of chloritoid thus calls for a revised approach of magnetic fabric interpretations in chloritoid-bearing rocks.

Citation: Haerinck, T., T. N. Debacker, and M. Sintubin (2013), Magnetic anisotropy of chloritoid, *J. Geophys. Res. Solid Earth*, *118*, 3886–3898, doi:10.1002/jgrb.50276.

1. Introduction

[2] The anisotropy of magnetic susceptibility (AMS) of a rock or sediment can serve as a useful tool when investigating the petrofabric. Whereas pioneering magnetic fabric studies focused on ferromagnetic fabrics [*Graham*, 1954; *Balsley and Buddington*, 1960; *Rees*, 1961; *Fuller*, 1964], it became soon clear that "matrix minerals", having a paramagnetic or diamagnetic behavior, often significantly contribute to the observed magnetic fabrics [*Coward and Whalley*, 1979; *Rochette and Vialon*, 1984; *Borradaile et al.*, 1986]. The last decades have seen an increased interest in magnetic (sub)fabrics carried by paramagnetic minerals [e.g., *Lüneburg et al.*, 1999; *Hirt et al.*, 2000; *Chadima et al.*, 2004; *Debacker et al.*, 2004; *Cifelli et al.*, 2005; *Debacker et al.*, 2009]. The intrinsic anisotropy of paramagnetic matrix minerals is dominantly a magnetocrystalline anisotropy in contrast to the intrinsic anisotropy of ferromagnetic (*s.l.*) minerals which may result from a combination of magnetostatic (shape), distribution (interaction), and magnetocrystalline anisotropy [*Borradaile and Jackson*, 2004]. This makes the paramagnetic (sub)fabric dependent on only two factors: first, the orientation distribution of the paramagnetic minerals and second, their intrinsic magnetocrystalline anisotropy. This magnetocrystalline anisotropy is related to atomic scale exchange interactions between the transition element ions, mainly Fe^{2+}, Fe^{3+}, and Mn^{2+}, which are anistropically distributed in the crystal lattice. Hence, the anisotropic exchange interactions define easy directions in the crystal lattice. This crystallographic control opens possibilities for the use of the paramagnetic AMS as a quantitative indicator of the degree of fabric development provided the intrinsic magnetic anisotropy of all individual minerals present is known.

[3] The intrinsic AMS of a single (paramagnetic) mineral can be determined by measurements on large, natural or synthetic, single crystals or on assemblages of strongly oriented grains. As natural single minerals often contain ferromagnetic impurities [e.g., *Borradaile*, 1994; *Lagroix and Borradaile*, 2000; *Feinberg et al.*, 2005], such analyses should use an approach that allows isolating the paramagnetic, magnetocrystalline anisotropy [*Martín-Hernández*

Additional supporting information may be found in the online version of this article.

[1]Geodynamics and Geofluids Research Group, Department of Earth and Environmental Sciences, KU Leuven, Leuven, Belgium.
[2]FROGTECH Ltd., Deakin, ACT, Australia.

Corresponding author: T. Haerinck, Geodynamics and Geofluids Research Group, Department of Earth and Environmental Sciences, KU Leuven, Celestijnenlaan 200E, BE-3001 Leuven, Belgium. (tom.haerinck@ees.kuleuven.be)

2169-9313/13/10.1002/jgrb.50276

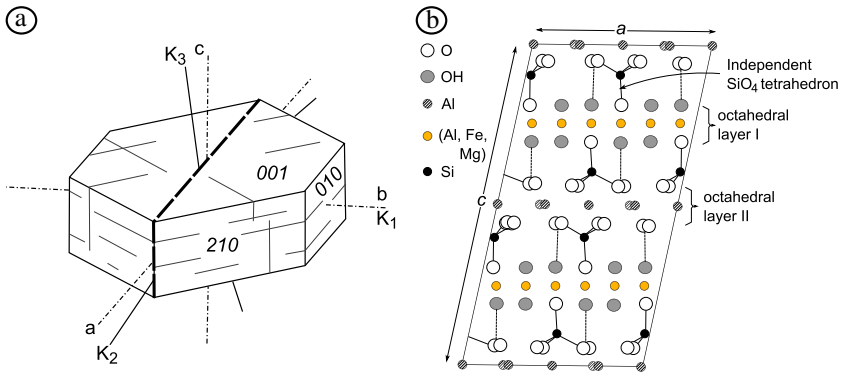

Figure 1. (a) Chloritoid crystal showing a possible arrangement of the crystallographic controlled principal susceptibility axes. (b) Projection of the monoclinic chloritoid structure on (010). Octahedral layer I has a composition of $[Fe^{2+}{}_2AlO_2(OH)_4]^-$ with some Mg^{2+} and Mn^{2+} substituting for Fe^{2+}, octahedral layer II has the composition of $[Al_3O_8]^{7-}$ and isolated SiO_4 tetrahedra link these layers (redrawn after *Klein et al*. [2002]).

and Ferré, 2007]. Analyses of the mineral AMS have been carried out for common rock-forming, paramagnetic minerals like the Fe-bearing phyllosilicates biotite, muscovite, chlorite, and phlogopite [*Beausoleil et al*., 1983; *Borradaile et al*., 1987; *Zapletal*, 1990; *Borradaile and Werner*, 1994; *Martín-Hernández and Hirt*, 2003], the mafic silicates pyroxene, orthopyroxene, amphibole, and their alteration products serpentine and epidote [*Hrouda*, 1982; *Wiedenmann et al*., 1986; *Lagroix and Borradaile*, 2000], olivines [*Belley et al*., 2009], tourmaline [*Rochette et al*., 1992; *Lagroix and Borradaile*, 2000], and Fe-bearing carbonates [*Rochette*, 1988]. For all these Fe-bearing silicates, it was found that using the definition of *Jelinek* [1981], the degree of anisotropy (P_J) does not exceed 1.35. After *Rochette* [1987] and *Rochette et al*. [1992], the P_J value of 1.35 has therefore been used as the upper limit for the paramagnetic contribution to the AMS in siliciclastic rocks. Higher P_J values are to date systematically attributed to a ferromagnetic (*s.l*.) contribution [e.g., *Gil-Imaz and Barbero*, 2004; *Aïfa and Idres*, 2010; *Amrouch et al*., 2010; *Hrouda*, 2010].

[4] However, in a recent magnetic fabric study of Armorican metasediments, *Haerinck et al*. [2013] encountered a dominantly paramagnetic anisotropy with P_J values up to 1.45 for epizonal, chloritoid, and white mica-bearing siltstones. Anchizonal, chlorite, and white mica-bearing siltstones of the same stratigraphic horizon, though, show only P_J values up to 1.27. These observations suggest that the intrinsic AMS of chloritoid may be significantly higher than that of phyllosilicates and other Fe-bearing silicates. Moreover, the upper limit of 1.35 for a paramagnetic contribution to the AMS seems not applicable for these chloritoid-bearing siltstones.

[5] In order to test this hypothesis, this study presents an analysis of the magnetocrystalline anisotropy on a collection of chloritoid single crystals by means of two independent high-field approaches. The ferromagnetic (*s.l*.) impurities in the chloritoid crystals are characterized in order to assess whether these phases saturate in the applied fields and the used approaches are valid. By determining the paramagnetic, magnetocrystalline anisotropy of chloritoid, the study verifies whether chloritoid-bearing rocks can have a paramagnetic anisotropy that exceeds the 1.35 limit of *Rochette* [1987] as inferred by *Haerinck et al*. [2013]. Furthermore, the values of the intrinsic AMS of chloritoid, presented in this work, can be used for modeling the magnetic fabric of chloritoid-bearing rocks. These models can help to get a more complete understanding of the origin of the magnetic anisotropy in these rocks and will facilitate quantitative interpretation [e.g., *Hrouda and Schulmann*, 1990; *Siegesmund et al*., 1995; *de Wall et al*., 2000; *Martín-Hernández et al*., 2005].

2. The Mineral Chloritoid

[6] Chloritoid is a relatively common mineral in aluminum-rich, metapelitic rocks both from lower greenschist to amphibolites facies conditions and from HP blueschist to eclogite facies conditions. It is a hydrous Fe-Al nesosilicate mineral with an ideal formula of $Fe^{2+}{}_2Al_4O_2(SiO_4)_2(OH)_4$. Chloritoid is monoclinic and has a layered structure consisting of two different octahedral layers and sheets of isolated SiO_4 tetrahedra (Figure 1) [*Klein et al*., 2002]. Octahedral layer I (brucite type) consists of two planes of O^{2-} and $(OH)_2^-$ with Fe^{2+} in two thirds of the octahedral sites and Al^{3+} in the remaining octahedral sites. Mg^{2+} and Mn^{2+} may replace up to about 68% and 50% of the Fe^{2+}, respectively, although most of the chloritoid is relatively Fe rich. Octahedral layer II (corundum type) consists of two planes of O^{2-} with three fourths of the octahedral sites occupied by Al^{3+} or Fe^{3+}. This makes the structure of chloritoid very similar to that of the phyllosilicates, except for the $SiO_4{}^{4-}$ tetrahedra which are not bond together as in the case of the phyllosilicates. Crystals are usually platy, parallel to (001) with a roughly hexagonal basal section.

[7] The paramagnetic susceptibility of chloritoid is due to magnetic moments associated with spin motion of unpaired electron in the 3d orbitals of the $Fe^{2+/3+}$ and Mn^{2+} cations that become partially aligned in the presence of an external magnetic field. This "pure paramagnetic" behavior is modified by weak exchange coupling and electrostatic interactions between the magnetic cations. As the magnetic cations are anisotropically distributed, i.e., they are dominantly positioned in the brucite-type octahedral layers, the strength and nature of the magnetic interactions, which are expressed by the Weiss temperature (θ), should be expected to vary (systematically) with orientation in the lattice. Hence, these weak exchange interactions will give rise to the magnetocrystalline anisotropy of chloritoid [*Borradaile and Jackson*, 2004].

3. The Chloritoid Crystals

[8] A collection of seven chloritoid single crystals (Ctd01–Ctd07) has been analyzed. The crystals have been cut into 18 cubic specimens with variable dimensions, ranging from 2 mm to 7.15 mm. The specimens are oriented with the *x* and *y* directions chosen arbitrarily and perpendicular to each other within the basal plane and the *z* direction perpendicular to the basal plane. After the analyses, a smaller "daughter" specimen—denoted with an asterisk—is cut from five relatively large specimens, i.e., Ctd01A*, Ctd01B*, Ctd05A*, Ctd05B*, and Ctd07A*. These daughter specimens will be analyzed in order to assess the accuracy of the approach. The crystals originate from five different localities:

[9] 1. Ctd01 and Ctd02 are from Ness of Hillswick in the northwest Shetland Mainland, UK. The crystals are a constituent of metapelites from the Early Neoproterozoic Sand Voe group, which can be correlated to the Moine metasediments in Scotland, UK. Chloritoid was formed due to Caledonian Barrovian-type metamorphism in upper greenschist facies conditions [*Fettes*, 1979];

[10] 2. Ctd03 is taken from Carboniferous metapelites of the Narragansett basin in Natick, Rhode Island, USA. Similar to Ctd01 and Ctd02, it was formed due to Barrovian-type metamorphism in upper greenschist facies conditions, associated with the Alleghanian orogeny [*Murray et al*., 2004];

[11] 3. Ctd04 is from Permian metapelites of the Sierra de los Filabres, Andalucia, Spain. Neoformation of the chloritoid crystals was due to greenschist facies Alpine metamorphism [*Vissers*, 1977];

[12] 4. Ctd05 and Ctd06 originate from the village of St. Marcel in the Aosta valley, Italy, and occur in hydrothermally altered metabasalts of the Zermatt-Saas ophiolite. The ophiolite has been subjected to subduction-related HP-metamorphism in eclogite facies conditions (21 ± 3 kbar, 550°C) during the Alpine orogeny [*Angiboust et al*., 2009];

[13] 5. Ctd07 is from Île de Groix, France. It occurs in micaschists and metabasites with an Ordovician protolith age that have been subjected to Variscan, blueschist facies HP-metamorphism (18 ± 2 kbar, 500°C) [*Bosse et al*., 2002].

4. Methodology

4.1. Characterization of the Ferromagnetic (*s.l.*) Inclusions

[14] As the high-field approaches require the ferromagnetic (*s.l.*) phases in the chloritoid specimens to saturate below the maximum applied field, it is necessary to characterize these phases and determine whether they comply with this requirement. The remanent magnetization (M_r), the saturation magnetization (M_s), and the coercivity (B_c) of the ferromagnetic (*s.l.*) phases present can be derived from the ferromagnetic component of a magnetic hysteresis loop, at least if this ferromagnetic loop is significant, meaning that it has a quality factor Q_f of at least 1. This Q_f is defined as the logarithm of the signal/noise ratio. Magnetic hysteresis loops are measured with a vibrating sample magnetometer (VSM), applying a maximum field of 1 T in 10 mT increments. The ferromagnetic loops are obtained by subtracting the linear (paramagnetic) contribution from the measured loop. A more thorough characterization of the ferromagnetic (*s.l.*) phases present in the chloritoid specimens is obtained from magnetic remanence experiments, as remanence measurements are not influenced by the dominant paramagnetic behavior of the chloritoid host. Two different types of magnetic remanence experiments have been made: first, alternating field (AF) demagnetization of isothermal remanent magnetization (IRM) and of anhysteretic remanent magnetization (ARM) and second, low-temperature cycling of a saturation isothermal remanent magnetization (SIRM).

[15] In the AF demagnetization experiment, an IRM of 1 T and an ARM of 200 mT are acquired and subsequently stepwise demagnetized in 15 steps from 5 to 200 mT using a Schonstedt AF demagnetizer. The remanent magnetization after each step is measured with a 2G superconducting rock magnetometer. The shape of the demagnetization curve and the intensity of the IRM or ARM are dependent on the amount and type of ferromagnetic (*s.l.*) phases. The field required to reduce the initial remanence by one half is called the median destructive field (MDF). Both IRM and ARM demagnetization are performed as these different methods can activate dissimilar remanence coercivity fractions, and a comparison of both demagnetization curves has some diagnostic potential [*Lowrie and Fuller*, 1971].

[16] The SIRM experiment comprises cycling a 2.5 T room temperature (300 K) SIRM (RT-SIRM) down to 10 K and back to room temperature in zero field, while the remanence is monitored with a Quantum Design Magnetic Properties Measuring System (MPMS). The RT-SIRM behavior during the low-temperature cycle can be attributed to a temperature-dependent behavior of the common, natural ferromagnetic (*s.l.*) phases, i.e., magnetite [*Halgedahl and Jarrard*, 1995; *Özdemir and Dunlop*, 1999; *Dunlop*, 2003], maghemite [*Özdemir and Dunlop*, 2010], greigite [*Dekkers et al*., 2000], goethite [*Dekkers and Rochette*, 1992; *Maher et al*., 2004; *Liu et al*., 2006], hematite [*Özdemir and Dunlop*, 2006], and pyrrhotite [*Besnus*, 1966; *Fillion and Rochette*, 1988; *Wolfers et al*., 2011]. If the presence of goethite is suspected from the RT-SIRM low-temperature cycling experiment, this is additionally verified by comparing the thermal demagnetization to room temperature of a 2.5 T SIRM acquired at 10 K after zero field cooling (ZFC) with a 2.5 T SIRM acquired during cooling, i.e., field cooling (FC). Goethite typically shows a much stronger FC M_r than a ZFC M_r at low temperatures.

4.2. Magnetic Anisotropy Analyses

[17] Two independent high-field approaches have been used for determining the paramagnetic, magnetocrystalline anisotropy of the chloritoid single crystals. The first approach uses a VSM, applying a maximum field of 1 T and 10 mT increments, to generate a magnetic hysteresis loop successively in 24 directions, i.e., 45° rotation increments around the three orthogonal axes of the specimen. The high-field magnetic susceptibility (κ^{hf}) is defined in each direction as the slope of a linear fit of the high-field part of the loop (i.e., >600, 700, or 800 mT depending on the correlation coefficient). The HF-AMS^{VSM} tensor is calculated using the same software that processes standard low-field AMS data. A detailed outline of the approach is given in *Kelso et al*. [2002], with some improvements in *Ferré et al*. [2004]. The accuracy of the VSM approach is assessed by comparing the obtained result for five specimens (Ctd01A-B, Ctd05A-B, and Ctd07A) with that of a small daughter specimen, denoted with an asterisk, which is cut out of the original specimen.

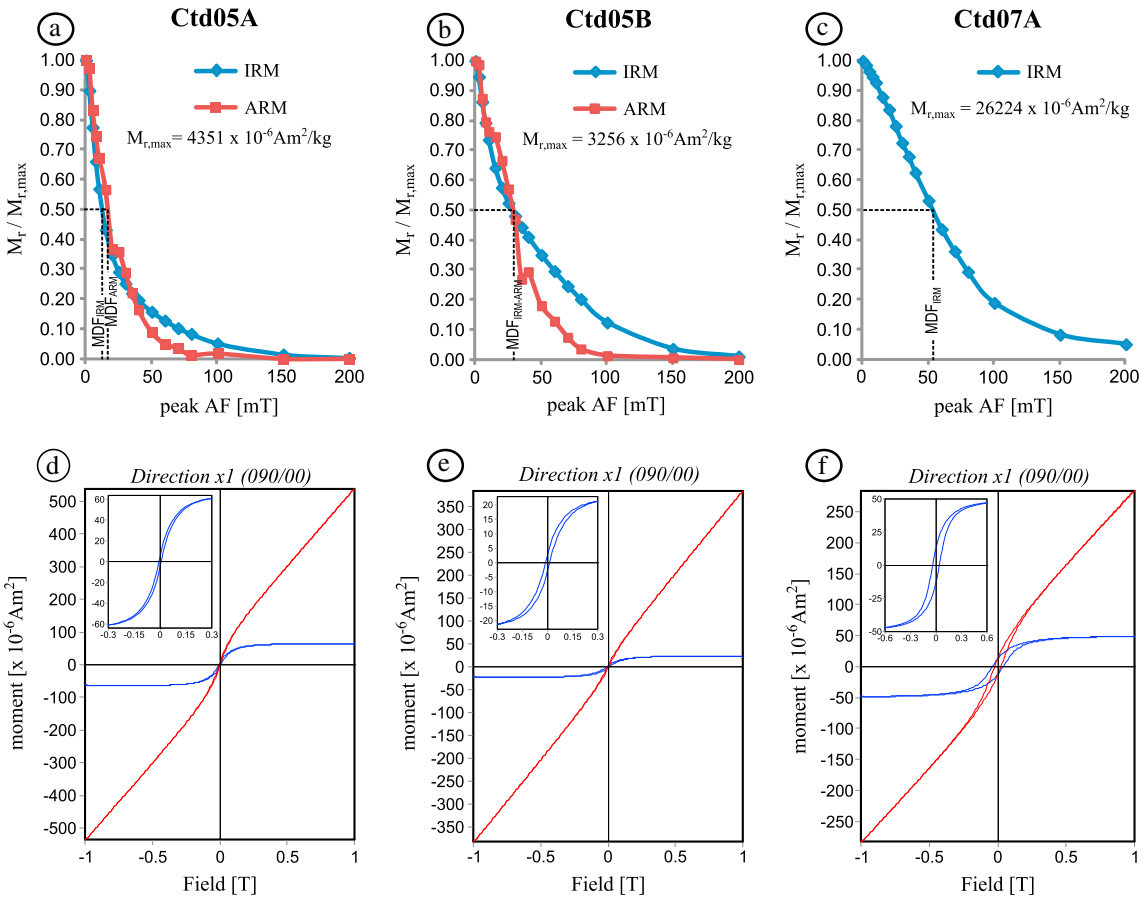

Figure 2. (a–c) Alternating-field demagnetization of a 1 T isothermal remanent magnetization (IRM) (blue curve) and a 200 mT anhysteretic remanent magnetization (ARM) (red curve). The median destructive field of the IRM and ARM ($MDF^{IRM/ARM}$) is the field required to demagnetize half of the original IRM and ARM, respectively. (d–f) The red curves are the measured magnetic hysteresis in the *y* direction of the specimen, i.e., within the basal plane. The blue curves show the ferromagnetic loops, obtained after paramagnetic correction.

Inconsistencies in the HF-AMS^{VSM} of a "mother-daughter couple" can be seen as an indication of the inaccuracy of the approach due to shape effects and/or misorienting of the sometimes very small specimens.

[18] The second high-field approach uses a torsion magnetometer [*Bergmuller et al.*, 1994], which directly measures the torque exerted by the specimen hanging in an applied field with its easy axis not exactly parallel, antiparallel, or perpendicular to the applied field. Torsion measurements are performed at 36 positions, i.e., 30° rotation increments around the three orthogonal axes of the specimen, and in six magnetic fields ranging from 700 to 1500 mT. These data are processed in order to isolate the paramagnetic contribution to the specimen's magnetic susceptibility and determine its deviatoric susceptibility tensor using a mathematical technique developed by *Martín-Hernández and Hirt* [2001]. Next, we use the mean susceptibility of the HF-AMS^{VSM} approach, i.e., the bulk susceptibility K_m^{hf}, and add this to the deviatoric tensor in order to calculate the full paramagnetic tensor (HF-AMS^{torque}).

[19] Both HF-AMS tensors can be represented by an ellipsoid with principal axes $K_1^{VSM/torque} > K_2^{VSM/torque} > K_3^{VSM/torque}$. The magnetic anisotropy ellipsoid is described by two parameters. First, the corrected degree of anisotropy $P_J^{VSM/torque}$ reflects the eccentricity of the ellipsoid. Second, the shape parameter $T^{VSM/torque}$ is used to discriminate between prolate ($T < 0$) and oblate ($T > 0$) ellipsoids [*Jelinek*, 1981]. The orientation of the magnetic anisotropy ellipsoid with respect to the basal plane is expressed by the inclination angle of the minimum susceptibility axis with the basal plane I-$K_3^{VSM/torque}$. As the hysteresis data also allow a computation of M_r in the different measurement positions (at least if the ferromagnetic component is significant), also the anisotropy of isothermal remanent magnetization (AIRM) tensor can be calculated. The AIRM can be described by the same parameters as the HF-AMS tensors.

[20] Finally, the exchange interactions which cause the magnetocrystalline anisotropy are characterized by defining the Weiss temperature (θ)—also called the paramagnetic Curie temperature—and the Curie constant (C) for the chloritoid crystals. This is done both in an orientation parallel ($C/\theta^{\parallel}$) and perpendicular ($C/\theta^{\perp}$) to the basal plane. In order todo this, κ^{hf} is analyzed in function of temperature by performing hysteresis measurements at 18 temperatures between 300 and 10 K. The hysteresis measurements are carried out with a Quantum Design MPMS and applying a

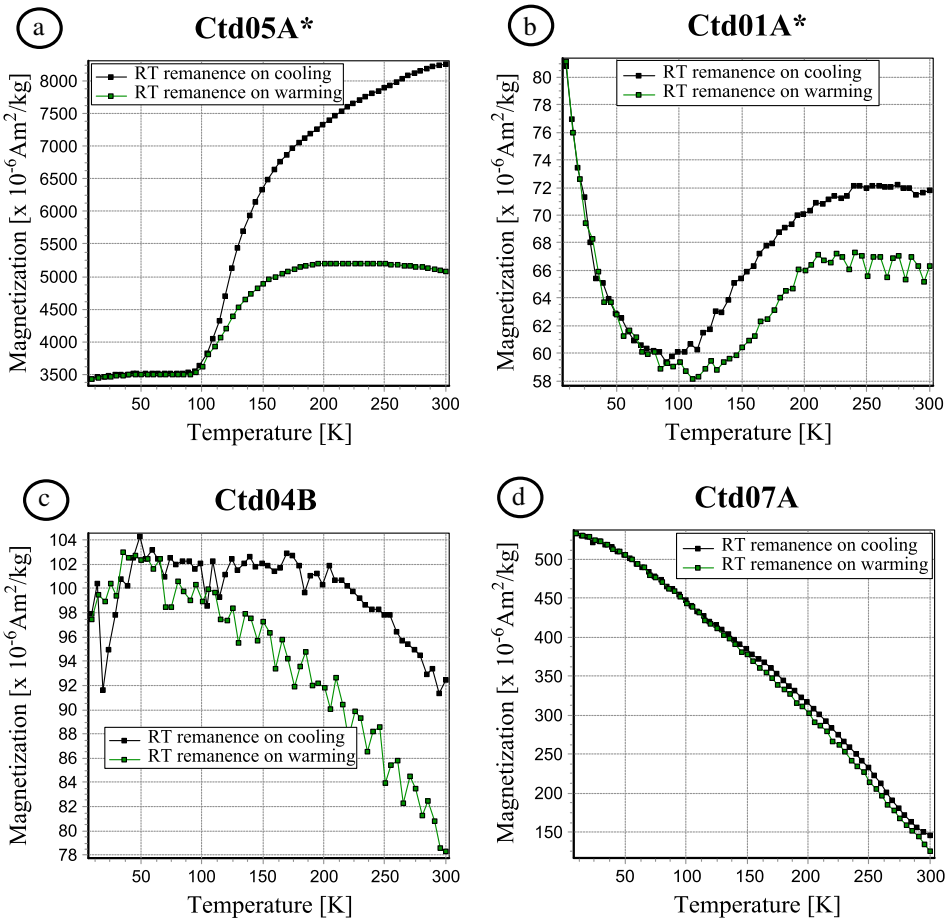

Figure 3. Results of the low-temperature cycling of saturation isothermal remanent magnetization (SIRM) acquired at room temperature in a field of 2.5 T. The remanence upon cooling is shown in black and that upon reheating in green.

maximum field of 2.5 T. A plot of the reciprocal κ^{hf} to temperature allows the derivation of C, i.e., the reciprocal of the slope of the linear part of the curve, and θ, i.e., the temperature-axis intercept of an extrapolation of the linear part of the curve. θ tells us below which temperature magnetic ordering takes place (i.e., the exchange interaction is not overcome by thermal motion) and is a measure of the nature and strength of the interactions between the magnetic ions. Values of $\theta > 0$ K indicate ferromagnetic interactions and $\theta < 0$ K indicate weak, antiferromagnetic interactions [*Borradaile and Jackson*, 2004].

5. Characterization of the Ferromagnetic Inclusions

[21] All specimens do show a measurable magnetic remanence, and thus contain ferromagnetic (*s.l.*) inclusions. Text S1 in the supporting information gives an overview of the results of the magnetic remanence experiments and a hysteresis loop for all 18 specimens. For most specimens, the remanence is relatively weak with a 1 T IRM generally below 220×10^{-6} Am^2/kg. Three specimens (Ctd05C, Ctd06A, and Ctd07B) have a slightly higher 1 T IRM with values between 422 and 672×10^{-6} Am^2/kg. Ctd05A and Ctd05B and especially Ctd07A show a clearly more pronounced magnetic remanence with a 1 T IRM of 4351 and 3256×10^{-6} Am^2/kg for the Ctd05 specimens and $26{,}224 \times 10^{-6}$ Am^2/kg for Ctd07A. The IRM demagnetization curves of Ctd05A and Ctd05B show an initially steep drop with half the original magnetization already lost after 13 and 16 mT demagnetization, respectively, i.e., the median destructive field (MDF) (Figures 2a and 2b). Demagnetization of the ARM shows a very similar pattern and MDF. The IRM demagnetization of Ctd07A shows a more moderate drop with a MDF of 54 mT (Figure 2c). Its ARM falls immediately within a noise level (not shown in the figure). The hysteresis loop of specimens Ctd05A and Ctd05B contains a strong paramagnetic component, but with a clear deviation from the linear trend around the zero field (Figures 2d and 2e). The ferromagnetic loop is characterized by a small difference between the upper and lower hysteresis branch. The coercivity of the ferromagnetic (*s.l.*) phase is relatively low, i.e., 7 and 12 mT, respectively, just as the ratio of M_r to M_s, i.e., 0.07 and 0.10, respectively. These observations indicate a soft ferromagnetic (*s.l.*) phase. Also, specimen Ctd07A shows a composite hysteresis loop arising from both a paramagnetic and a ferromagnetic (*s.l.*) component (Figure 2f). For this specimen, the difference between the upper and lower hysteresis branch is somewhat larger as evidenced by its coercivity and M_r to M_s ratio, i.e., 40 mT and 0.26, respectively, indicating a relatively harder ferromagnetic (*s.l.*) phase compared to the Ctd05 specimens. For all other specimens, the demagnetization curves fall

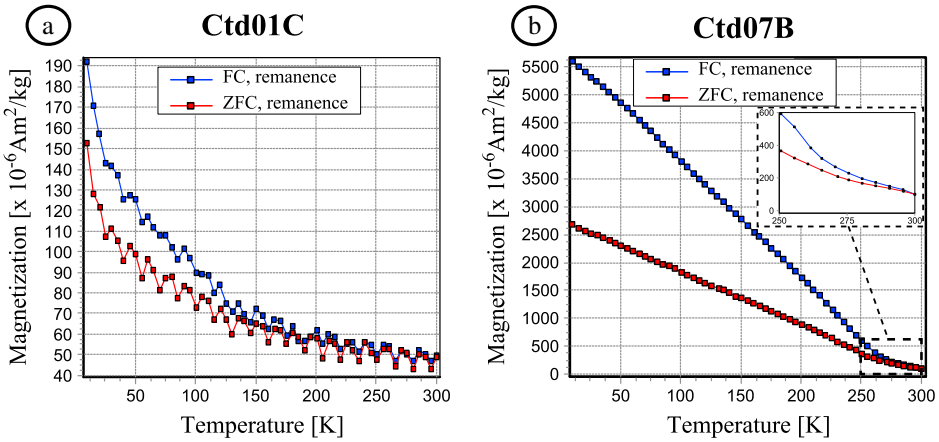

Figure 4. Comparison of thermal demagnetization to room temperature of a 2.5 T SIRM acquired at 10 K, i.e., zero field cooling (ZFC), shown as the red curve, to the demagnetization of a 2.5 T SIRM acquired during cooling from room temperature to 10 K, i.e., field cooling (FC), shown as the blue curve.

relatively fast in the noise level, often already at 0.20 M_r/M_{rmax} for the IRM demagnetization and immediately at M_{rmax} for theARM demagnetization for which only an inducing field of 200 mT could be used. Also, the ferromagnetic hysteresis loops (obtained after paramagnetic correction) have a low signal/noise ratio (figures in Text S1). This leaves the low-temperature cycling of the SIRM, measured on the more sensitive MPMS, as the best tool to characterize the ferromagnetic mineralogy for these specimens.

[22] The specimens of crystals Ctd01, Ctd02, Ctd03, Ctd04, Ctd05, and Ctd06 all show a very similar behavior of the RT-SIRM during low temperature cycling, although the magnitude of the remanence can vary. During cooling, a significant loss in remanence takes place roughly between 200 and 100 K. At very low temperatures, from 100 to 10 K, the remanence may drift a bit, either with a positive or a negative trend, due to additional (paramagnetic) magnetization induced by an imperfect zero field in the MPMS. Upon reheating, the remanence is more or less reversible until approximately 100 to 130 K; from then onward, a clear loss in remanence with respect to the situation during cooling is apparent (Figures 3a–3c). The amount of recovery of the remanence lost upon cooling ranges between 30% and 50%. For specimen Ctd01C, the thermal demagnetization to room temperature of a low-temperature FC and ZFC remanence is compared (Figure 4a). The FC remanence is slightly stronger at low temperature: The FC/ZFC ratio at 10 K is 1.26. Upon heating, the difference gradually decreases and disappears around 120 K. The remanence behavior at low temperature of these specimens is indicative for the presence of magnetite, which goes through the Verwey phase transition at approximately $T_V \sim 120$ K. The RT-SIRM cooling curve of specimen Ctd04B shows also a pronounced drop at 35–30 K, which breaks the positive trend that likely arises from magnetization induced by an imperfect zero field (Figure 3c). This drop indicates the presence of pyrrhotite that goes through the Besnus phase transition at 32 K [*Fillion and Rochette*, 1988]. Ctd04B is the only specimen that shows this phenomenon.

[23] The specimens of crystal Ctd07 show a completely different behavior of the RT-SIRM during low-temperature cycling. The remanence is inversely related to temperature: Upon cooling from 300 to 10 K, the remanence increases by a factor of 4 to 6. The remanence decreases perfectly reversible upon reheating back to room temperature for specimen Ctd07B (Figure 3d) and up to approximately 130 K for specimens Ctd07A and Ctd07C, which show from then onward a slightly lower remanence compared to the situation before cooling. Comparison of the thermal demagnetization to room temperature of low-temperature FC and ZFC remanence for specimen Ctd07B shows a FC/ZFC remanence ratio at 10 K of 2 that gradually decreases upon heating but is persistent up to 300 K (Figure 4b). This behavior is indicative of goethite, which is far from being saturated by the 2.5 T field. The small remanence difference between the cooling and heating curve for specimens Ctd07A and Ctd07C above T_V indicates that also some magnetite is present in these specimens.

6. Results of the Magnetic Anisotropy Analyses

[24] The high-field bulk susceptibility (K_m^{hf}/χ^{hf}) is listed in Table 1 for all 18 specimens together with the magnitude of the principal axes and the P_J, T, and I-K_3 parameter of both the HF-AMS^{VSM} (derived from directional hysteresis measurements) and the HF-AMS^{torque} (derived by means of torque magnetometry). The HF-AMS^{VSM} ellipsoid shows for all specimens a very oblate shape with most specimens having a T^{VSM} value above 0.90. P_J^{VSM} ranges between 1.34 and 1.54. There are notable differences in P_J^{VSM} from crystal to crystal. The specimens of crystal Ctd02 and Ctd03 have a noticeable lower P_J^{VSM} value than the specimens from the other crystals. Those of crystals Ctd04, and to a lesser extent Ctd01, have a somewhat higher P_J^{VSM} than the average value. As for the orientation of the high-field principal susceptibility axes, I-K_3^{VSM} shows an average value of 85 ± 02. This means that K_1^{VSM} and K_2^{VSM} are roughly contained within the basal plane and K_3^{VSM} is approximately normal to the basal plane. A comparison of these results with the daughter specimen for five specimens is shown in Table 2. K_m^{hf} shows very similar values for all five specimens, suggesting a rather homogeneous $Fe^{2+/3+}$ and Mn^{2+} distribution in the crystals. K_1^{VSM}, K_2^{VSM}, and K_3^{VSM}, and consequently also P_J^{VSM} and T^{VSM}, again show very small differences between the mother and daughter

Table 1. Bulk Susceptibility and High-Field AMS Properties (VSM and Torque Approach) of the Chloritoid Specimens[a]

	Bulk Susceptibility		HF-AMS^{VSM}						HF-AMS^{torque}						ΔVSM^{torque}		
Name	χ^{hf} (m^3/kg)	K_m^{hf} [SI]	K_1^{VSM}	K_2^{VSM}	K_3^{VSM}	P_J^{VSM}	T^{VSM}	I-K_3^{VSM}	K_1^{torque}	K_2^{torque}	K_3^{torque}	P_J^{torque}	T^{torque}	I-K_3^{torque}	ΔP_J	ΔT	ΔI-K_3
Ctd01A	41×10^{-8}	1398×10^{-6}	1.117	1.108	0.776	1.52	0.95	86°									
Ctd01A*	43×10^{-8}	1429×10^{-6}	1.112	1.104	0.784	1.49	0.96	86°	1.114	1.106	0.781	1.50	0.96	83°	0.01	0.00	3°
Ctd01B	43×10^{-8}	1508×10^{-6}	1.111	1.106	0.782	1.50	0.97	85°									
Ctd01B*	42×10^{-8}	1463×10^{-6}	1.113	1.104	0.783	1.49	0.95	82°	1.107	1.100	0.794	1.46	0.96	88°	0.03	0.01	6°
Ctd01C	42×10^{-8}	1587×10^{-6}	1.116	1.106	0.778	1.51	0.95	86°	1.114	1.103	0.783	1.49	0.94	90°	0.01	0.01	4°
Ctd02A	45×10^{-8}	1599×10^{-6}	1.102	1.074	0.824	1.38	0.82	86°	1.106	1.071	0.822	1.39	0.78	89°	0.00	0.04	3°
Ctd03A	54×10^{-8}	2612×10^{-6}	1.081	1.079	0.840	1.34	0.98	85°	1.084	1.077	0.838	1.34	0.95	88°	0.00	0.03	4°
Ctd04A	45×10^{-8}	1865×10^{-6}	1.123	1.110	0.767	1.54	0.94	88°	1.122	1.110	0.768	1.54	0.94	89°	0.00	0.00	1°
Ctd04B	55×10^{-8}	1650×10^{-6}	1.117	1.110	0.773	1.53	0.97	88°	1.116	1.111	0.773	1.52	0.98	88°	0.00	0.01	0°
Ctd04C	55×10^{-8}	2162×10^{-6}	1.120	1.111	0.769	1.54	0.96	88°	1.114	1.112	0.774	1.52	0.99	87°	0.02	0.03	1°
Ctd05A	45×10^{-8}	1525×10^{-6}	1.113	1.099	0.787	1.48	0.93	88°									
Ctd05A*	44×10^{-8}	1508×10^{-6}	1.108	1.101	0.791	1.47	0.96	86°	1.108	1.102	0.789	1.48	0.97	82°	0.00	0.01	4°
Ctd05B	44×10^{-8}	1517×10^{-6}	1.104	1.097	0.799	1.45	0.96	85°									
Ctd05B*	41×10^{-8}	1524×10^{-6}	1.102	1.083	0.815	1.46	0.89	82°	1.100	1.087	0.813	1.41	0.92	83°	0.05	0.03	1°
Ctd05C	46×10^{-8}	1579×10^{-6}	1.120	1.103	0.777	1.51	0.92	83°	1.110	1.106	0.783	1.49	0.98	85°	0.02	0.06	1°
Ctd06A	46×10^{-8}	1551×10^{-6}	1.112	1.103	0.785	1.49	0.95	79°	1.109	1.101	0.790	1.47	0.96	77°	0.02	0.01	2°
Ctd06B	47×10^{-8}	1592×10^{-6}	1.108	1.077	0.815	1.41	0.82	86°	1.112	1.080	0.807	1.43	0.82	85°	0.02	0.00	1°
Ctd06C	47×10^{-8}	1572×10^{-6}	1.113	1.108	0.779	1.51	0.97	85°	1.113	1.105	0.783	1.50	0.96	84°	0.01	0.01	1°
Ctd06D	47×10^{-8}	1651×10^{-6}	1.120	1.107	0.772	1.53	0.94	85°	1.120	1.113	0.766	1.54	0.97	83°	0.02	0.03	2°
Ctd07A	51×10^{-8}	1806×10^{-6}	1.113	1.093	0.795	1.46	0.89	86°									
Ctd07A*	53×10^{-8}	1777×10^{-6}	1.110	1.099	0.791	1.46	0.94	80°	1.105	1.094	0.800	1.44	0.94	86°	0.02	0.01	6°
Ctd07B	55×10^{-8}	2031×10^{-6}	1.110	1.099	0.791	1.47	0.94	73°	1.108	1.100	0.791	1.47	0.96	76°	0.00	0.02	3°
Ctd07C	54×10^{-8}	1927×10^{-6}	1.107	1.100	0.793	1.46	0.97	83°	1.106	1.100	0.795	1.46	0.97	79°	0.00	0.00	4°
mean[†]	48×10^{-8}	1726×10^{-6}	1.111	1.100	0.789	1.48	0.94	85°	1.109	1.099	0.792	1.47	0.94	85°	0.01	0.02	3°
	$\pm 6 \times 10^{-8}$	$\pm 301 \times 10^{-6}$	± 0.010	± 0.013	± 0.022	± 0.06	± 0.05	± 2°	± 0.008	± 0.012	± 0.019	± 0.05	± 0.05	± 4°	± 0.01	± 0.02	± 2°

[a]High-field bulk susceptibility derived from the vibrating sample magnetometer approach (χ^{hf} is the mass susceptibility and K_m^{hf} the volume susceptibility) and from both the HF-AMS determined with the VSM approach (denoted with superscript VSM) and the HF-AMS determined with the torque approach (denoted with superscript torque). The mean values of the different parameters and their standard deviations are calculated using the specimens of crystals Ctd01, Ctd02, Ctd03, Ctd04, Ctd05, and Ctd06, and discarding those of crystal Ctd07. K_1, K_2, and K_3 are the principal magnetic susceptibilities, P_J is the corrected degree of anisotropy [*Jelinek*, 1981], T is the shape parameter [*Jelinek*, 1981], and I-K_3 is the inclination angle between the minimum susceptibility axis and the basal plane.

Table 2. HF-AMS Properties of the Daughter Specimens and Absolute Differences With Their Respective Mother Specimens[a]

	HF-AMS^{VSM}							Absolute Difference Mother-Daughter Specimen						
Name	$K_m{}^{hf}$ [SI]	$K_1{}^{VSM}$	$K_2{}^{VSM}$	$K_3{}^{VSM}$	$P_J{}^{VSM}$	T^{VSM}	I-$K_3{}^{VSM}$	$\Delta K_m{}^{hf}$ [SI]	$K_1{}^{VSM}$	$K_2{}^{VSM}$	$K_3{}^{VSM}$	$P_J{}^{VSM}$	T^{VSM}	I-$K_3{}^{VSM}$
Ctd01A*	1429×10^{-6}	1.112	1.104	0.784	1.49	0.96	86°	31×10^{-6}	0.005	0.003	0.008	0.02	0.01	1°
Ctd01B*	1463×10^{-6}	1.113	1.104	0.783	1.49	0.95	82°	45×10^{-6}	0.002	0.003	0.000	0.00	0.02	3°
Ctd05A*	1508×10^{-6}	1.108	1.101	0.791	1.47	0.96	86°	17×10^{-6}	0.005	0.002	0.004	0.01	0.04	2°
Ctd05B*	1524×10^{-6}	1.102	1.083	0.815	1.46	0.89	82°	7×10^{-6}	0.003	0.013	0.016	0.01	0.07	3°
Ctd07A*	1777×10^{-6}	1.110	1.099	0.791	1.46	0.94	80°	29×10^{-6}	0.003	0.007	0.004	0.00	0.05	6°
							mean	26×10^{-6} $\pm 14 \times 10^{-6}$	0.004 ± 0.005	0.006 ± 0.006	0.006 ± 0.010	0.01 ± 0.01	0.04 ± 0.02	3° ± 2°

[a]The table shows the HF-AMS results of the five daughter specimens together with the absolute difference in HF-AMS parameters between the daughter specimens and the original specimen from which it has been cut.

specimens. The largest mother-daughter difference in $P_J{}^{VSM}$ occurs in Ctd01A, i.e., 0.025 or 1.65%. When looking at T^{VSM}, the largest difference occurs in Ctd05B, i.e., 0.069 or 7.78%. Also, I-$K_3{}^{VSM}$ shows limited differences between mother and daughter specimens, with 6° as largest difference (Ctd07A).

[25] The highly oblate high-field anisotropy, $T^{VSM} = 0.94 \pm 0.05$, and the direction of $K_1{}^{VSM}$ and $K_2{}^{VSM}$ within the basal plane suggest a quasi-isotropic susceptibility within the basal plane. In order to check this in more detail, κ^{hf} has been determined as a function of orientation within the basal plane, with measurements every 10° for all specimens. The maximum deviation of κ^{hf} from the mean value for the basal plane (i.e., the radius of a best fit circle) ranges between 0.74% (specimen Ctd06C) and 2.81% (specimen Ctd02A) (Table 3). It is not possible to distinguish whether this deviation is due to a magnetic anisotropy within the basal plane or to a misorientation during cutting the specimen and/or placing it in the VSM. However, any anisotropy in the basal plane must be very small, i.e., not more than a few percent. The κ^{hf} measurements in the function of orientation within the basal plane, together with a plot showing the residual value between the best fit circle and the measured κ^{hf} in the function of orientation within the basal plane, are shown in Text S2.

[26] Figure 5 shows the results of the high-field torque analysis for representative specimen Ctd01A*. The relatively high amplitude of the torque function for rotation positions 1 and 2 indicates a strong tendency of the specimen to rotate itself with the easy axis parallel to the applied field at these measurement positions, i.e., those with an angle of 45° between the inducing field and the specimen's basal plane. A detailed overview of the torsion measurements and the obtained deviatoric tensors of the paramagnetic contribution for all specimens investigated is given in Text S3. For each specimen, the deviatoric susceptibility tensor is added to $K_m{}^{hf}$, determined with the VSM, in order to obtain the full HF-AMS^{torque} tensor. The HF-AMS^{torque} ellipsoids have a high degree of anisotropy ($P_J{}^{torque}$ values between 1.34 and1.54), are very oblate (most specimens have a T^{torque} value above 0.90), and are roughly parallel to the basal plane (I-$K_3{}^{torque}$ shows an average value of 85° ± 4°) (Table 1). The absolute differences between both HF-AMS approaches (ΔP_J, ΔT, and ΔI-K_3) are generally very low, displaying maximum values of 0.05 for P_J, 0.06 for T, and 6° for I-K_3 (Table 1).

[27] Four specimens show significant ferromagnetic loops, allowing the AIRM to be calculated (Table 4). The $P_J{}^{IRM}$ values found for the Ctd05 specimens range from 1.49 to 1.63, which is somewhat higher than the $P_J{}^{hf}$ values, and the shape of the remanent magnetization ellipsoid is again rather oblate with T^{hf} ranging from 0.47 to 0.89. $K_3{}^{IRM}$ makes a high angle with the basal plane, i.e., I-$K_3{}^{IRM}$ is between 75° and 88°. The AIRM of specimen Ctd07A has a significantly lower $P_J{}^{IRM}$ and has a distinctly prolate remanent magnetization ellipsoid with $K_3{}^{IRM}$ oriented at a low angle to the basal plane. For specimens Ctd01C and Ctd06D, κ^{hf} within the basal plane is determined as a function of temperature from 300 to 10 K (Figures 6a and 6b). On a plot of the reciprocal κ^{hf} to temperature, a linear behavior is observed from 300 to approximately 60 K, whereas lower temperatures show an increasing upward deviation from the linear trend. This deviation is related to assumptions, used for deriving the Curie-Weiss law, that are no longer valid close to the paramagnetic Curie temperature θ due to strong fluctuations of the magnetic moments. The data obtained for $1/\kappa^{hf}$ above 60 K have been processed by the least squares method, giving a value of 0.49 and 0.54, respectively, for $C^{\parallel}$ and 6.0 K and 4.4 K, respectively, for $\theta^{\parallel}$. The positive values for $\theta^{\parallel}$ indicate the presence of ferromagnetic exchange interactions within the basal plane. Magnetic ordering will only take place below this temperature. For specimen Ctd01C, also κ^{hf} perpendicular to the basal plane is determined as function of temperature (Figure 6c). The plot of the reciprocal

Table 3. High-Field Magnetic Susceptibility in the Chloritoid Basal Plane[a]

Name	Mean BP-κ^{hf} [SI]	Max. Deviation
Ctd01A	1507×10^{-6}	1.19%
Ctd01B	1592×10^{-6}	2.07%
Ctd01C	1780×10^{-6}	1.41%
Ctd02A	1757×10^{-6}	2.81%
Ctd03A	2845×10^{-6}	1.35%
Ctd04A	2080×10^{-6}	1.30%
Ctd04B	1842×10^{-6}	1.53%
Ctd04C	2387×10^{-6}	1.37%
Ctd05A	1721×10^{-6}	2.14%
Ctd05B	1673×10^{-6}	2.51%
Ctd05C	1779×10^{-6}	1.60%
Ctd06A	1683×10^{-6}	2.15%
Ctd06B	1757×10^{-6}	2.42%
Ctd06C	1747×10^{-6}	0.74%
Ctd06D	1914×10^{-6}	1.39%
Ctd07A	1987×10^{-6}	1.95%
Ctd07B	2240×10^{-6}	2.03%
Ctd07C	2128×10^{-6}	1.09%

[a]The table shows the mean high-field magnetic susceptibility obtained by measuring the high-field susceptibility with 10° increments in the basal plane of the chloritoid specimens, and the maximum deviation of the mean value displayed by a single measurement.

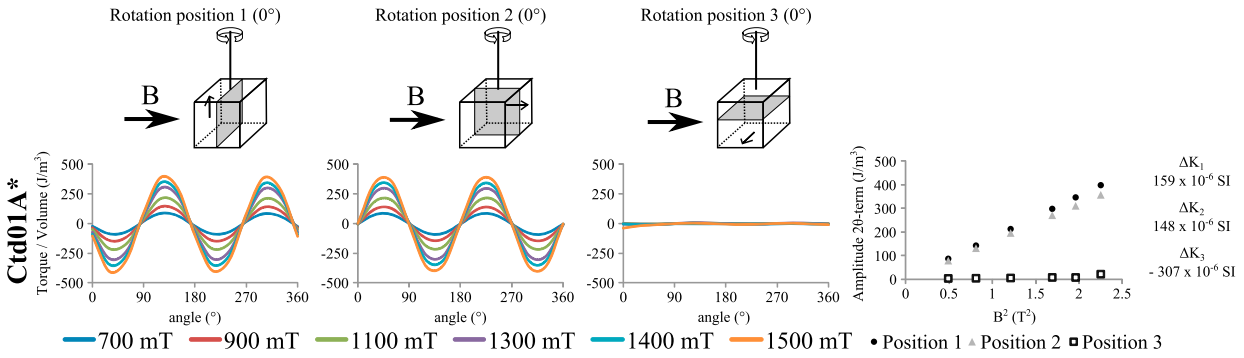

Figure 5. Results of the high-field torque analysis for specimen Ctd01A*. Rotation positions 1 and 2 (around an orthogonal axis in the basal plane) show a well-defined periodical function with maximum and minimum values at approximately 45°, 135°, 225°, and 315°, i.e., when the angle between the inducing field and the specimen's basal plane is 45°. Rotation position 3 (around the orthogonal axis perpendicular to the basal plane) shows hardly any torque signal. The plot on the right shows the amplitude of the periodical torque function as a function of the inducing magnetic field squared (B^2) for the three measurement positions. The calculated deviatoric eigenvalues (ΔK_1, ΔK_2, and ΔK_3), i.e., the absolute difference between the mean susceptibility and the principal susceptibilities, are given on the far right.

κ^{hf} to the temperature permits a value of 0.40 to be determined for $C^{\perp}$ and −35.6 K for $\theta^{\perp}$. The negative value of $\theta^{\perp}$ indicates an antiferromagnetic coupling between the planes.

7. Discussion

[28] Magnetic remanence experiments reveal that ferromagnetic (*s.l.*) impurities, made up of magnetite, are present in the specimens of crystals Ctd01, Ctd02, Ctd03, Ctd04, Ctd05, and Ctd06. Specimen Ctd04B seems to contain also some pyrrhotite. The low M_r/M_s ratio and coercivity obtained from the ferromagnetic hysteresis loops of the Ctd05 specimens are indicative of multidomain magnetite. Magnetite is a relatively soft ferrimagnetic mineral, certainly when it consists of multidomain particles, and also a major part of pyrrhotite gets magnetized in a field of 600 mT [*Peters and Dekkers*, 2003]. Hence, the high-field approach allows the separation of the paramagnetic, magnetocrystalline anisotropy of chloritoid from the contribution of the ferromagnetic (*s.l.*) impurities. For the three specimens of crystal Ctd07, the magnetic remanence experiments show the presence of goethite. Because goethite is a hard, antiferromagnetic mineral that does not reach saturation in a field of 1 T [*Peters and Dekkers*, 2003], the goethite impurities will contribute to κ^{hf} and the HF-AMS does not uniquely reflect the magnetocrystalline anisotropy of chloritoid. However, the goethite-bearing Ctd07 specimens do show similar $P_J^{VSM/torque}$ and $T^{VSM/torque}$ values as the other specimens. This may suggest that a major part of the goethite impurities does saturate and will not contribute to κ^{hf}. Nevertheless, we have chosen not to use the Ctd07 specimens for determining the magnetocrystalline anisotropy of chloritoid.

[29] The HF-AMS has been determined using two independent high-field approaches that deliver mutually very consistent results. By reevaluating the obtained HF-AMS^{VSM} of five daughter specimens cut out of the original specimens and comparing them to the values of the original specimen, we have assessed possible inaccuracies of our approach due to shape effects and slight misorientations. The observed differences in P_J^{VSM} and T^{VSM} between "mother" and daughter specimens are very small, i.e., maximum 0.02 and 0.07, respectively, indicating that the obtained results are not significantly biased by shape effects or orientation irregularities. The high-field degree of anisotropy obtained for chloritoid is $P_J = 1.47 \pm 0.06$ with some differences between the different crystals, and the shape of the high-field susceptibility ellipsoid is highly oblate with $T = 0.94 \pm 0.06$ (average value of both approaches). A possible explanation for the slight variation in P_J between the crystals is that they may have a variable Fe and Mn cation content, as it was tentatively suggested for biotite single crystals by *Martín-Hernández and Hirt* [2003]. However, this is contradicted by a plot of $P_J^{VSM/torque}$ to K_m^{hf} that does not show an apparent relationship (Figure 7). Still, we cannot discard the possibility that a variable Fe^{2+}/Fe^{3+} ratio influences the degree of anisotropy.

[30] All specimens have $K_3^{VSM/torque}$ oriented approximately perpendicular to the basal plane (Table 1) and $K_1^{VSM/torque}$ and $K_2^{VSM/torque}$ roughly contained within the basal plane, arguing for a strong correspondence between

Table 4. AIRM Results for the Relevant Chloritoid Specimens[a]

Name	$M_{r\text{-}mean}$ (Am^2/kg)	K_1^{IRM}	K_2^{IRM}	K_3^{IRM}	P_J^{IRM}	T^{IRM}	I-K_3^{IRM}
Ctd05A	3362×10^{-6}	1.140	1.114	0.746	1.61	0.89	88°
Ctd05B	2630×10^{-6}	1.161	1.096	0.743	1.63	0.74	75°
Ctd05C	566×10^{-6}	1.161	1.049	0.790	1.49	0.47	83°
Ctd07A	25387×10^{-6}	1.113	0.959	0.928	1.21	−0.64	8°

[a]The table shows the anisotropy of isothermal remanent magnetization (AIRM), denoted with superscript IRM, for the four specimens with a reliable ferromagnetic hysteresis component on a vibrating sample magnetometer.

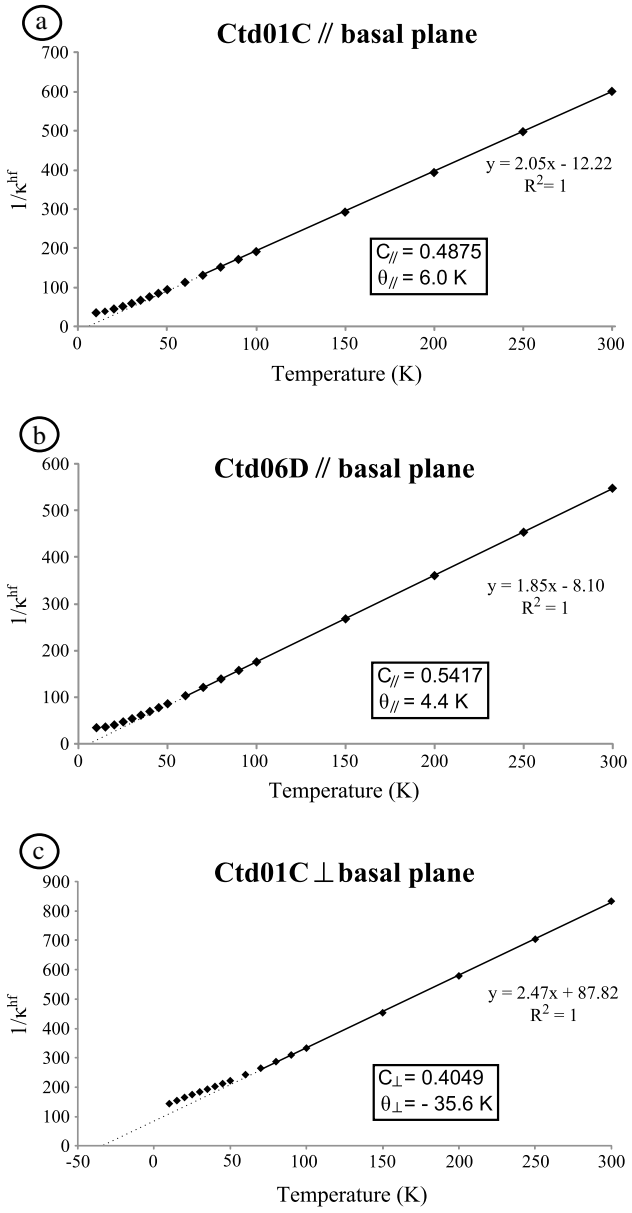

Figure 6. (a, b) Reciprocal of the magnetic susceptibility as a function of temperature measured within the basal plane. (c) Reciprocal of the magnetic susceptibility as a function of temperature measured perpendicular to the basal plane, i. e. parallel to the crystallographic c-axis.

the crystal habit and the HF-AMS. Unfortunately, chloritoid has a monoclinic crystallography whereas the principal κ^{hf} axes are orthogonal. Therefore, only one principal κ^{hf} axis is corresponding to a crystal axis, i.e., $K_1^{VSM/torque}$ which corresponds to the b-axis, and $K_2^{VSM/torque}$ and $K_3^{VSM/torque}$ are inclined with respect to the closest crystal axis (Figure 1) [*Borradaile and Jackson*, 2010]. However, these angular discrepancies are small for the tabular chloritoid crystals and within the accuracy of the specimen preparation and $K_3^{VSM/torque}$ is subparallel to the crystallographic c-axis. As for $K_1^{VSM/torque}$ and $K_2^{VSM/torque}$, the additional measurements carried out in the basal plane with the VSM approach and the very low torsion amplitude while rotating the specimens in the basal plane (Text S2) demonstrate that κ^{hf} is almost isotropic within the basal plane and it is not possible to determine whether the observed anisotropy of a maximum few percent is due to a real magnetic anisotropy in the basal plane or due to a misorientation. Hence, the exact direction of $K_1^{VSM/torque}$ and $K_2^{VSM/torque}$ in the basal plane cannot be established within the accuracy of the approach.

[31] From those samples where the ferromagnetic hysteresis loops are statistically significant, the three Ctd05 specimens have an AIRM that shows a close correspondence to the HF-AMS, i.e., the shape of the remanence ellipsoid is rather oblate and K_3^{IRM} is roughly perpendicular to the basal plane. This may indicate that the magnetite phases mimic the chloritoid lattice [cf. *Trindade et al*., 2001]. For the goethite component in specimen Ctd07A, this correspondence is lacking. However, given that K_3^{IRM} is almost oriented within the basal plane—instead of being oriented perpendicular to it—and the fact that goethite is known for generating inverse fabrics [*Dekkers and Rochette*, 1992], also the goethite phases may have nucleated in the direction of the chloritoid lattice.

[32] Taking into account the observed $P_J^{VSM/torque}$ values and the obtained accuracy range, it becomes clear that the degree of magnetocrystalline anisotropy in chloritoid single crystals is significantly higher than that of biotite, muscovite, and chlorite single crystals (Figure 8) [e.g., *Borradaile and Werner*, 1994; *Martín-Hernández and Hirt*, 2003]. It is also higher than the 1.35 upper limit of paramagnetic contribution to the AMS in siliciclastic rocks suggested by *Rochette* [1987] and *Rochette et al*. [1992]. In chloritoid, the number of Fe^{2+} cations is similar or lower than the number of Fe^{2+} in other paramagnetic minerals. Furthermore, our data show no link between P_J^{hf} and K_m^{hf} (Figure 7). This implies that the total Fe (and Mn) cation content does not govern the degree of anisotropy. So the remarkably high magnetic anisotropy of chloritoid is not simply the result of more Fe (and Mn) cations and hence, a stronger ferrimagnetic interaction within the basal plane. This is also confirmed by a comparison of the paramagnetic Curie temperature within the basal plane ofchloritoid, i.e., $\theta^{\parallel} = 5.2$ K (this study) and biotite, i.e., $\theta^{\parallel} = 22.7$ K [*Martín-Hernández*, 2002] and $\theta^{\parallel} = 27.4$ K [*Beausoleil et al*., 1983]. However, our analysis of κ^{hf} in function of temperature perpendicular to the basal plane shows that

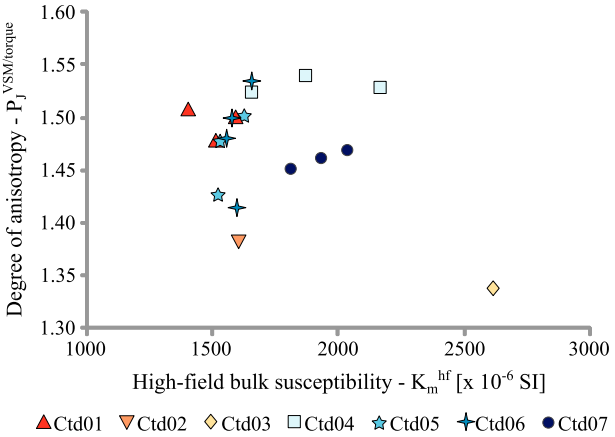

Figure 7. Plot of the high-field bulk susceptibility to the high-field degree of anisotropy (average value of VMS and torque approach) for the different chloritoid specimens, showing no apparent correlation.

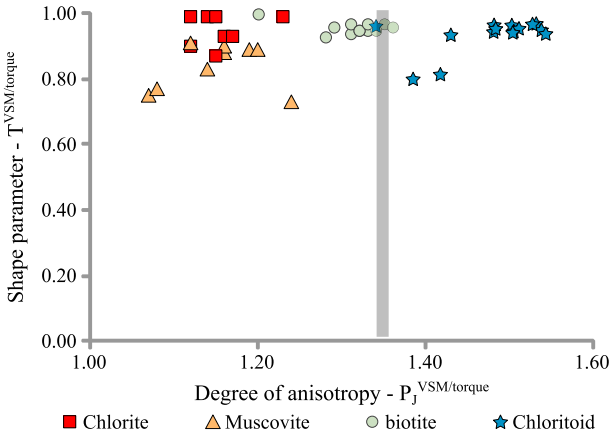

Figure 8. Jelinek plot of the high-field anisotropy magnetic susceptibility for single crystals of chloritoid (this study, average of VSM and torque approach), compared to chlorite, muscovite, and biotite [*Martín-Hernández and Hirt*, 2003]. The grey line corresponds to the frequently used upper limit (i.e., 1.35) for the paramagnetic.

the antiferromagnetic exchange interaction between the planes is strong in chloritoid, i.e., $\theta^{\perp} = -35.6$ K, whereas it is much weaker for biotite, for which *Martín-Hernández* [2002] and *Beausoleil et al*. [1983] obtained values of only $\theta^{\perp} = -13.5$ and $\theta^{\perp} = -6.8$ K, respectively. Therefore, based on the currently available data, we suggest that the relatively high magnetocrystalline anisotropy of chloritoid with respect to biotite is due to a strong antiferromagnetic interaction perpendicular to the basal plane.

8. Conclusion

[33] The magnetocrystalline anisotropy of chloritoid is successfully determined by means of two independent, but mutually very consistent, high-field approaches on a collection of 15 specimens coming from six single crystals, i.e., Ctd01, Ctd02, Ctd03, Ctd04, Ctd05, and Ctd06. These specimens contain magnetite impurities and possibly some pyrrhotite for specimen Ctd04B that saturate below 1 T and thus can be separated from the paramagnetic component by the high-field approach. The three specimens of single crystal Ctd07 contain a high coercivity, goethite phase and have been discarded from this analysis, since their HF-AMS may not uniquely reflect the magnetocrystalline anisotropy of chloritoid.

[34] The high-field susceptibility ellipsoid of chloritoid is highly oblate, with $T^{hf} = 0.94$, and has a minimum principal axis subparallel to the crystallographic c-axis of chloritoid, i.e., I-$K_3^{hf} = 85°$. Within the accuracy of the approach, the high-field magnetic susceptibility can be considered isotropic in the basal plane. The average degree of anisotropy obtained for chloritoid is $P_J^{hf} = 1.47$. This is significantly higher than high-field values obtained for the different phyllosilicates, biotite, muscovite, and chlorite, and is also higher than the 1.35 upper limit of paramagnetic contribution to AMS in siliciclastic rocks suggested by *Rochette* [1987] and *Rochette et al*. [1992]. The obtained values for θ indicate that this pronounced magnetocrystalline anisotropy is related to strong antiferromagnetic exchange interactions in the direction of the crystallographic c-axis ($\theta^{\perp} < 0$) and rather weak ferromagnetic exchange interactions within the basal plane ($\theta^{\parallel} > 0$). As a consequence, chloritoid-bearing rocks with a pronounced mineral alignment can have a paramagnetic anisotropy that significantly exceeds this limit, without the need of invoking strongly anisotropic, ferromagnetic minerals. The newly discovered magnetocrystalline anisotropy of chloritoid thus calls for a revised approach of magnetic fabric interpretations in chloritoid-bearing rocks.

[35] **Acknowledgments.** The work benefited a lot of the fruitful discussions with M. Jackson concerning the high-field anisotropy measurements and the low temperature behavior of the ferromagnetic minerals. The authors thank A. M. Hirt for providing us the opportunity to use the torsion magnetometer of the Laboratory for Natural Magnetism of ETH Zürich. We are indebted to G. J. Borradaile and an anonymous reviewer for their suggestions which improved the manuscript. Furthermore, the authors gratefully acknowledge John Faithfull, A. Weil, K. Linthout, A. M. Hirt, and M. Ballèvre for providing us with the chloritoid single crystals. Crystal Ctd01 came from the collection of the Hunterian Museum of the University of Glasgow (museum specimen number GLAHM 148189) and crystal Ctd03 is from the Bryn Mawr College Theodore Rand Mineral Collection. The research is financially supported by research grant G.0376.09N of the FWO-Vlaanderen, Belgium, and an Institute for Rock Magnetism (University of Minnesota) visiting fellowship for T.H. The IRM visiting fellowship was made possible through the Instrumentation and Facilities program of the National Science Foundation, Earth Science Division, and by funding from the University of Minnesota.

References

Aïfa, T., and M. Idres (2010), Indentation model using gravity anomaly and anisotropy of magnetic susceptibility: Consequences on nappe rotations in the Chélif Basin, Algeria, *Open Geol. J.*, *4*, 105–116.

Amrouch, K., P. Robion, J. P. Callot, O. Lacombe, J. M. Daniel, N. Bellahsen, and J. L. Faure (2010), Constraints on deformation mechanisms during folding provided by rock physical properties: A case study at Sheep Mountain anticline (Wyoming, USA), *Geophys. J. Int.*, *182*(3), 1105–1123, doi:10.1111/j.1365-246X.2010.04673.x.

Angiboust, S., P. Agard, L. Jolivet, and O. Beyssac (2009), The Zermatt-Saas ophiolite: The largest (60-km wide) and deepest (c. 70–80 km) continuous slice of oceanic lithosphere detached from a subduction zone?, *Terra Nova*, *21*(3), 171–180, doi:10.1111/j.1365-3121.2009.00870.x.

Balsley, J. R., and A. F. Buddington (1960), Magnetic susceptibility and fabric of some Adirondack granites and orthogneisses, *Am. J. Sci.*, *258*, 6–20.

Beausoleil, N., P. Lavallee, A. Yelon, O. Ballet, and J. M. D. Coey (1983), Magnetic properties of biotite micas, *J. Appl. Phys.*, *54*(2), 906–915, doi:10.1063/1.332053.

Belley, F., E. C. Ferré, F. Martín-Hernández, M. J. Jackson, M. D. Dyar, and E. J. Catlos (2009), The magnetic properties of natural and synthetic (Fe_x, $Mg_{1-x})_2$ SiO_4 olivines, *Earth Planet. Sci. Lett.*, *284*(3–4), 516–526, doi:10.1016/j.epsl.2009.05.016.

Bergmuller, F., C. Barlocher, B. Geyer, M. Grieder, F. Heller, and P. Zweifel (1994), A torque magnetometer for measurements of the high-field anisotropy of rocks and crystals, *Meas. Sci. Technol.*, *5*, 1466–1470, doi:10.1088/0957-0233/5/12/007.

Besnus, M. J. (1966), Propriétés magnétiques de la pyrrhotine naturelle, PhD thesis, University of Strasbourg, Strasbourg, France.

Borradaile, G. J. (1994), Paleomagnetism carried by crystal inclusions: The effect of preferred crystallographic orientation, *Earth Planet. Sci. Lett.*, *126*(1–3), 171–182, doi:10.1016/0012-821x(94)90249-6.

Borradaile, G. J., and M. Jackson (2004), Anisotropy of magnetic susceptibility (AMS): Magnetic petrofabrics of deformed rocks, *Geol. Soc. London, Spec. Publ.*, *238*(1), 299–360, doi:10.1144/GSL.SP.2004.238.01.18.

Borradaile, G. J., and M. Jackson (2010), Structural geology, petrofabrics and magnetic fabrics (AMS, AARM, AIRM), *J. Struct. Geol.*, *32*(10), 1519–1551, doi:10.1016/j.jsg.2009.09.006.

Borradaile, G. J., and T. Werner (1994), Magnetic anisotropy of some phyllosilicates, *Tectonophysics*, *235*(3), 223–248, doi:10.1016/0040-1951(94)90196-1.

Borradaile, G., J. Mothersill, D. Tarling, and C. Alford (1986), Sources of magnetic susceptibility in a slate, *Earth Planet. Sci. Lett.*, *76*(3–4), 336–340, doi:10.1016/0012-821X(86)90084-1.

Borradaile, G., W. Keeler, C. Alford, and P. Sarvas (1987), Anisotropy of magnetic susceptibility of some metamorphic minerals, *Phys. Earth Planet. In.*, *48*(1–2), 161–166, doi:10.1016/0031-9201(87)90119-1.

Bosse, V., M. Ballèvre, and O. Vidal (2002), Ductile thrusting recorded by the garnet isograd from blueschist-facies metapelites of the Ile de Groix,

Armorican Massif, France, *J. Petrol.*, *43*(3), 485–510, doi:10.1093/petrology/43.3.485.

Chadima, M., A. Hansen, A. M. Hirt, F. Hrouda, and H. Siemes (2004), Phyllosilicate preferred orientation as a control of magnetic fabric: Evidence from neutron texture goniometry and low and high-field magnetic anisotropy (SE Rhenohercynian Zone of Bohemian Massif), *Geol. Soc. London, Spec. Publ.*, *238*(1), 361–380, doi:10.1144/GSL.SP.2004.238.01.19.

Cifelli, F., M. Mattei, M. Chadima, A. M. Hirt, and A. Hansen (2005), The origin of tectonic lineation in extensional basins: Combined neutron texture and magnetic analyses on "undeformed" clays, *Earth Planet. Sci. Lett.*, *235*(1–2), 62–78, doi:10.1016/j.epsl.2005.02.042.

Coward, M. P., and J. S. Whalley (1979), Texture and fabric studies across the Kishorn Nappe, near Kyle of Lochalsh, Western Scotland, *J. Struct. Geol.*, *1*(4), 259–273, doi:10.1016/0191-8141(79)90001-4.

de Wall, H., M. Bestmann, and K. Ullemeyer (2000), Anisotropy of diamagnetic susceptibility in Thassos marble: A comparison between measured and modeled data, *J. Struct. Geol.*, *22*(11–12), 1761–1771, doi:10.1016/S0191-8141(00)00105-X.

Debacker, T. N., P. Robion, and M. Sintubin (2004), The anisotropy of magnetic susceptibility (AMS) in low-grade, cleaved pelitic rocks: Influence of cleavage/bedding angle and type and relative orientation of magnetic carriers, *Magn. Fab.: Methods and Appl.*, *238*, 77–77, doi:10.1144/GSL.SP.2004.238.01.08.

Debacker, T. N., A. M. Hirt, M. Sintubin, and P. Robion (2009), Differences between magnetic and mineral fabrics in low-grade, cleaved siliciclastic pelites: A case study from the Anglo-Brabant Deformation Belt (Belgium), *Tectonophysics*, *466*(1–2), 32–46, doi:10.1016/j.tecto.2008.09.039.

Dekkers, M. J., and P. Rochette (1992), Magnetic properties of chemical remanent magnetization in synthetic and natural goethite: Prospects for a natural remanent magnetization/thermoremenant magnetization ratio paleomagnetic stability test?, *J. Geophys. Res.*, *97*(B12), 17,291-217,307–217,291-217,307, doi:10.1029/92JB01026.

Dekkers, M. J., H. F. Passier, and M. A. A. Schoonen (2000), Magnetic properties of hydrothermally synthesized greigite (Fe_3S_4)—II. High- and low-temperature characteristics, *Geophys. J. Int.*, *141*(3), 809–819, doi:10.1046/j.1365-246x.2000.00129.x.

Dunlop, D. J. (2003), Stepwise and continuous low-temperature demagnetization, *Geophys. Res. Lett.*, *30*, 4–4, doi:10.1029/2003GL017268.

Feinberg, J. M., G. R. Scott, P. R. Renne, and H.-R. Wenk (2005), Exsolved magnetite inclusions in silicates: Features determining their remanence behavior, *Geology*, *33*(6), 513–516, doi:10.1130/g21290.1.

Ferré, E. C., F. Martín-Hernández, C. Teyssier, and M. Jackson (2004), Paramagnetic and ferromagnetic anisotropy of magnetic susceptibility in migmatites: Measurements in high and low fields and kinematic implications, *Geophys. J. Int.*, *157*(3), 1119–1129, doi:10.1111/j.1365-246X.2004.02294.x.

Fettes, D. J. (1979), A metamorphic map of the British and Irish Caledonides, *Geol. Soc. London,Spec. Publ.*, *8*(1), 305–321, doi:10.1144/gsl.sp.1979.008.01.35.

Fillion, G., and P. Rochette (1988), The low temperature transition in monoclinic pyrrhotite, *J. Phys. Colloque*, *C8*(49), 907–908, doi:10.1051/jphyscol:19888412.

Fuller, M. D. (1964), On the magnetic fabrics of certain rocks, *J. Geol.*, *72*(3), 368–376.

Gil-Imaz, A., and L. Barbero (2004), Anisotropy of magnetic susceptibility in the Montes de Toledo area (Hercynian Iberian Belt, Spain) and its petrostructural significance, *Geol. Soc. London,Spec. Publ.*, *238*(1), 381–394, doi:10.1144/gsl.sp.2004.238.01.20.

Graham, J. W. (1954), Magnetic susceptibility anisotropy, an unexploited petrofabric element, *Geol. Soc. Am. Bull.*, *65*(12), 1257–1258.

Haerinck, T., R. Adriaens, T. N. Debacker, A. M. Hirt, and M. Sintubin (2013), Paramagnetic metamorphic mineral assemblages controlling AMS in low-grade deformed metasediments and the implications with respect to the use of AMS as a strain marker, *J. Geol. Soc.*, *170*(2), 263–280, doi:10.1144/jgs2012-062.

Halgedahl, S. L., and R. D. Jarrard (1995), Low-temperature behavior of single-domain through multidomain magnetite, *Earth Planet. Sci. Lett.*, *130*(1–4), 127–139.

Hirt, A. M., M. Julivert, and J. Soldevila (2000), Magnetic fabric and deformation in the Navia-Alto Sil slate belt, northwestern Spain, *Tectonophysics*, *320*(1), 1–16, doi:10.1016/S0040-1951(00)00047-0.

Hrouda, F. (1982), Magnetic anisotropy of rocks and its application in geology and geophysics, *Surv. Geophys.*, *5*(1), 37–82, doi:10.1007/bf01450244.

Hrouda, F. (2010), Modelling relationship between bulk susceptibility and AMS in rocks consisting of two magnetic fractions represented by ferromagnetic and paramagnetic minerals—Implications for understanding magnetic fabrics in deformed rocks, *J. Geol. Soc. India*, *75*(1), 254–266, doi:10.1007/s12594-010-0013-0.

Hrouda, F., and K. Schulmann (1990), Conversion of the magnetic susceptibility tensor into the orientation tensor in some rocks, *Phys. Earth Planet. In.*, *63*(1–2), 71–77, doi:10.1016/0031-9201(90)90061-2.

Jelinek, V. (1981), Characterization of the magnetic fabric of rocks, *Tectonophysics*, *79*(3–4), 63–67, doi:10.1016/0040-1951(81)90110-4.

Kelso, P. R., B. Tikoff, M. Jackson, and W. Sun (2002), A new method for the separation of paramagnetic and ferromagnetic susceptibility anisotropy using low field and high field methods, *Geophys. J. Int.*, *151*(2), 345–359, doi:10.1046/j.1365-246X.2002.01732.x.

Klein, C., C. S. Hurlbut, and J. D. Dana (2002), *The 22nd Edition of theManual of Mineral Science (After James D. Dana)*, John Wiley, NewYork.

Lagroix, F., and G. J. Borradaile (2000), Magnetic fabric interpretation complicated by inclusions in mafic silicates, *Tectonophysics*, *325*(3–4), 207–225, doi:10.1016/s0040-1951(00)00125-6.

Liu, Q., Y. Yu, J. Torrent, A. P. Roberts, Y. Pan, and R. Zhu (2006), Characteristic low-temperature magnetic properties of aluminous goethite [α-(Fe, Al)OOH] explained, *J. Geophys. Res.*, *111*, B12S34, doi:10.1029/2006JB004560.

Lowrie, W., and M. Fuller (1971), On the alternating field demagnetization characteristics of multidomain thermoremanent magnetization in magnetite, *J. Geophys. Res.*, *76*(26), 6339-6349–6339–6349, doi:10.1029/JB076i026p06339.

Lüneburg, C. M., S. A. Lampert, H. D. Lebit, A. M. Hirt, M. Casey, and W. Lowrie (1999), Magnetic anisotropy, rock fabrics and finite strain in deformed sediments of SW Sardinia (Italy), *Tectonophysics*, *307*(1–2), 51–74, doi:10.1016/S0040-1951(99)00118-3.

Maher, B. A., V. V. Karloukovski, and T. J. Mutch (2004), High-field remanence properties of synthetic and natural submicrometre haematites and goethites: Significance for environmental contexts, *Earth Planet. Sci. Lett.*, *226*(3–4), 491–505.

Martín-Hernández, F. (2002), Determination of fundamental magnetic anisotropy parameters in rock-forming minerals and their contributions to the magnetic fabric of rocks, PhD thesis, ETH Zürich, Zürich, Switzerland.

Martín-Hernández, F., and E. C. Ferré (2007), Separation of paramagnetic and ferrimagnetic anisotropies: A review, *J. Geophys. Res.*, *112*, 16–16, doi:10.1029/2006JB004340.

Martín-Hernández, F., and A. M. Hirt (2001), Separation of ferrimagnetic and paramagnetic anisotropies using a high-field torsion magnetometer, *Tectonophysics*, 337(3-4), 209–221, doi:10.1016/j.tecto.2005.12.011.

Martín-Hernández, F., and A. M. Hirt (2003), The anisotropy of magnetic susceptibility in biotite, muscovite and chlorite single crystals, *Tectonophysics*, *367*(1–2), 13–28, doi:10.1016/S0040-1951(03)00127-6.

Martín-Hernández, F., K. Kunze, M. Julivert, and A. M. Hirt (2005), Mathematical simulations of anisotropy of magnetic susceptibility on composite fabrics, *J. Geophys. Res.*, *110*, 12–12, doi:10.1029/2004JB003505.

Murray, D. P., J. W. Skehan, and J. Raben (2004), Tectonostratigraphic relationships and coalification trends in the Narragansett and Norfolk Basins, New England, *J. Geodyn.*, *37*(3–5), 583–611, doi:10.1016/j.jog.2004.02.006.

Özdemir, Ö., and D. J. Dunlop (1999), Low-temperature properties of a single crystal of magnetite oriented along principal magnetic axes, *Earth Planet. Sci. Lett.*, *165*(2), 229–239.

Özdemir, Ö., and D. J. Dunlop (2006), Magnetic memory and coupling between spin-canted and defect magnetism in hematite, *J. Geophys. Res.*, *111*, B12S03, doi:10.1029/2006JB004555.

Özdemir, Ö., and D. J. Dunlop (2010), Hallmarks of maghemitization in low-temperature remanence cycling of partially oxidized magnetite nanoparticles, *J. Geophys. Res.*, *115*, B02101, doi:10.1029/2009JB006756.

Peters, C., and M. J. Dekkers (2003), Selected room temperature magnetic parameters as a function of mineralogy, concentration and grain size, *Phys. Chem. Earth Parts A/B/C*, *28*(16–19), 659–667, doi:10.1016/s1474-7065(03)00120-7.

Rees, A. I. (1961), The effect of water currents on the magnetic remanence and anisotropy of susceptibility of some sediments, *Geophys. J. Roy. Astron. Soc.*, *5*(3), 235–251, doi:10.1111/j.1365-246X.1961.tb00431.x.

Rochette, P. (1987), Magnetic susceptibility of the rock matrix related to magnetic fabric studies, *J. Struct. Geol.*, *9*(8), 1015–1020, doi:10.1016/0191-8141(87)90009-5.

Rochette, P. (1988), Inverse magnetic fabric in carbonate-bearing rocks, *Earth Planet. Sci. Lett.*, *90*(2), 229–237, doi:10.1016/0012-821x(88)90103-3.

Rochette, P., and P. Vialon (1984), Development of planar and linear fabrics in Dauphinois shales and slates (French Alps) studied by magnetic anisotropy and its mineralogical control, *J. Struct. Geol.*, *6*(1–2), 33–38, doi:10.1016/0191-8141(84)90081-6.

Rochette, P., M. Jackson, and C. Aubourg (1992), Rock magnetism and the interpretation of anisotropy of magnetic susceptibility, *Rev. Geophys.*, *30*(3), 209–226, doi:10.1029/92RG00733.

Siegesmund, S., K. Ullemeyer, and M. Dahms (1995), Control of magnetic rock fabrics by mica preferred orientation: A quantitative approach, *J. Struct. Geol.*, *17*(11), 1601–1613, doi:10.1016/0191-8141(95)00047-H.

Trindade, R. I. F., T. Mintsa Mi Nguema, and J. L. Bouchez (2001), Thermally enhanced mimetic fabric of magnetite in a biotite granite, *Geophys. Res. Lett.*, *28*(14), 2687–2690, doi:10.1029/2001GL013218.

Vissers, R. (1977), Data on the tectonic and metamorphic evolution of the central Sierra De Los Filabres, Betic Cordilleras, se Spain, *Geol. Rundsch.*, *66*(1), 81–90, doi:10.1007/bf01989565.

Wiedenmann, A., J. R. Regnard, G. Fillion, and S. S. Hafner (1986), Magnetic properties and magnetic ordering of the orthopyroxenes Fe_x Mg_{1-x} SiO_3, *J. Phys. C: Solid State Phys.*, *19*(19), 3683, doi:10.1088/0022-3719/19/19/022.

Wolfers, P., G. Fillion, B. Ouladdiaf, R. Ballou, and P. Rochette (2011), The pyrrhotite 32 K magnetic transition, *Solid State Phenom.*, *170*, 174–179.

Zapletal, K. (1990), Low-field susceptibility anisotropy of some biotite crystals, *Phys. Earth Planet. In.*, *63*(1–2), 85–97, doi:10.1016/0031-9201(90)90063-4.